

# Nonlinear Electro- and Magneto-Optic Effects related to Bennett Structures

D. Budker,<sup>1,2,\*</sup> D. F. Kimball,<sup>1</sup> S. M. Rochester,<sup>1</sup> and V. V. Yashchuk<sup>1</sup>

<sup>1</sup>*Department of Physics, University of California at Berkeley, Berkeley, California 94720-7300*

<sup>2</sup>*Nuclear Science Division, Lawrence Berkeley National Laboratory, Berkeley, California 94720*

(Dated: August 10, 2001)

Optical pumping of an atomic sample with narrow-band light can create sub-Doppler features, known as Bennett structures, in the velocity distribution of state populations. In the presence of static magnetic or electric fields, the corresponding sub-Doppler features in the index of refraction can cause nonlinear optical rotation and induced ellipticity of resonant light propagating through the atomic medium. Physical mechanisms causing Bennett-structure-related nonlinear electro- and magneto-optical effects are discussed in detail for transitions involving states with low angular momenta. Measurements of Bennett-structure-related nonlinear magneto-optical rotation and electric field-induced ellipticity for the Rb D2 line are performed and compared to density matrix calculations. The latter effect can be used for measuring electric fields applied to atoms.

PACS numbers: 33.55.Ad, 33.55.Be, 42.62.Fi, 33.55.Fi

## I. INTRODUCTION

Nonlinear magneto-optical rotation (NMOR), light-power-dependent rotation of the polarization plane of light in a magnetic field (reviewed in, e.g., Refs. [1, 2]), has been of recent interest for magnetometry [3, 4] and discrete symmetry tests in atomic systems [5–7]. When linearly-polarized light propagates through an atomic sample along the direction of a magnetic field (Faraday geometry) and its frequency is tuned to the vicinity of an atomic resonance, several nested, dispersively-shaped features can be observed in the magnetic field dependence of the rotation angle  $\varphi$  (Fig. 1). Maxima in the rotation occur at different magnetic field magnitudes  $B_{\max}$ , corresponding to relaxation rates  $\gamma \approx 2g\mu B_{\max}/\hbar$ , where  $g$  is the Landé factor (typically of the lower state) and  $\mu$  is the Bohr magneton. In a typical Doppler-broadened atomic vapor, the feature with the largest  $B_{\max}$  corresponds to the Doppler width,  $\Gamma_D$ , and is due to linear (to first order independent of light power) Faraday rotation (the Macaluso-Corbino effect [8]). The narrower nonlinear features can be attributed to two different physical processes [9]: (1) the formation of Bennett structures [10]—“peaks” and “holes” in the velocity distribution of atomic state populations—due to optical pumping, and (2) evolution of light-induced atomic polarization in the magnetic field (the coherence effects).  $B_{\max}$  for Bennett-structure-related (BSR) NMOR corresponds to the natural width of the atomic transition (typically  $\gamma/(2\pi) = 1\text{-}10$  MHz for allowed optical electric-dipole transitions).  $B_{\max}$  for coherence effects is determined by the rate of relaxation of Zeeman coherences for atoms interacting with the light. Such relaxation can occur, for example, due to the exit of polarized atoms from the laser beam and simultaneous entrance of unpolarized atoms (“transit” effect; see Fig. 1). The smallest  $B_{\max}$  for

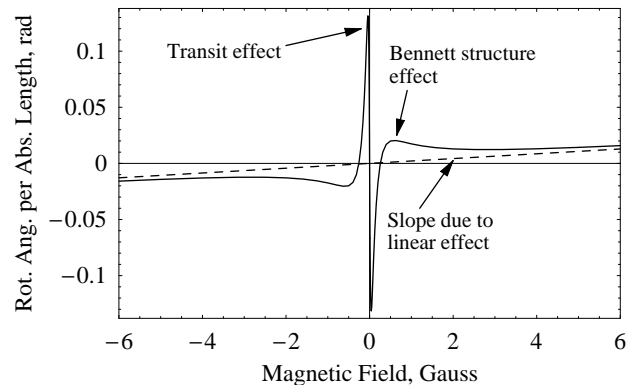


FIG. 1: Density matrix calculation of light polarization rotation as a function of magnetic field for the case of the samarium 571 nm line, under conditions of the experiment described in Ref. [9].

NMOR due to coherence effects ( $\sim 1$   $\mu\text{G}$ , corresponding to  $\gamma \approx 2\pi \times 1$  Hz) was achieved using antirelaxation coated vapor cells in Ref. [3]. While coherence effects in NMOR have been the subject of extensive investigation (see, e.g., Refs. [3, 4, 7, 11–13] and references therein), there have been limited studies of BSR NMOR (although it has been applied in laser frequency stabilization [14]). The present work contains the first explanation of the role of Bennett peaks in NMOR.

Although nonlinear electro-optic effects (NEOE) have been studied less extensively, they have been analyzed theoretically for  $1 \rightarrow 0$  and  $0 \rightarrow 1$  transitions [15, 16] and employed experimentally as a method for measuring atomic polarizabilities [15]. In this work, we perform the first detailed investigation of Bennett-structure-related NEOE, possible applications of which were discussed in Ref. [17]. This effect can be used for measuring electric fields applied to atoms. Here, we explore this application in the case of a paraffin-coated vapor cell with external electrodes.

\*Electronic address: budker@socrates.berkeley.edu

## II. PHYSICAL MECHANISMS OF BENNETT-STRUCTURE-RELATED NONLINEAR MAGNETO-OPTICAL EFFECTS

In order to elucidate the physical mechanisms which cause BSR NMOR, it is useful to separate the processes of *optical pumping* and *optical probing*. Optical pumping modifies the populations of and coherences between atomic states. Optical probing is the modification of the properties of light by interaction with the atomic medium. Note that if, as is the case in many experiments, a single laser beam is used for both pumping and probing, these processes occur simultaneously and continuously. However, comparison with full density matrix calculations and experiment shows that the essential features of BSR NMOR can be understood by considering these processes separately.

We thus consider BSR NMOR in the case of separated optical pumping and probing regions (Fig. 2), where different  $\hat{z}$ -directed magnetic fields ( $\mathbf{B}_{\text{pump}}$  and  $\mathbf{B}_{\text{probe}}$ , respectively) can be applied in the two regions. The atomic sample could be, e.g., a loosely collimated atomic beam traveling in the  $\hat{y}$ -direction with a broad transverse velocity (Doppler) distribution. (The desired magnetic field configuration can be realized in an experiment, e.g., with two side-by-side solenoids, with atoms traveling through a gap between the turns. The parameters can be arranged in such a way that the effect of the changing field between the regions is negligible.) In the pumping region, atoms interact with a near-resonant, linearly  $x$ -polarized, narrow band laser beam of saturating intensity (the optical pumping saturation parameter  $\kappa = d^2 E_0^2 / (\hbar^2 \gamma_0 \gamma_t) \gg 1$ , where  $d$  is the transition dipole moment,  $E_0$  is the optical electric field amplitude,  $\gamma_0$  is the natural width of the transition, and  $\gamma_t$  is the rate of atoms' transit through the pump laser beam). In the probing region, a weak ( $\kappa \ll 1$ ) light beam, initially of the same polarization as the pump beam, propagates through the medium. The resultant polarization of the probe beam is subsequently analyzed.

We will first consider an  $F = 1/2 \rightarrow F' = 1/2$  transition ( $F$  and  $F'$  are the total angular momenta of the ground and excited states, respectively). This system is especially straightforward, because it exhibits no coherence effect. Thus NMOR in this system is entirely due to Bennett structures. We will show that the mechanism of BSR depends critically on the details of the experimental situation. Depending on whether a magnetic field is present in the pump region, and whether the excited state decays to ground state or other levels, BSR NMOR can be due to holes, (and have one sign), be due to peaks (and have the opposite sign), or not be present at all.

Suppose first that the upper state decays to levels other than the ground state, and that  $\mathbf{B}_{\text{pump}} = 0$  [Fig. 3 (a)]. For atoms in the resonant velocity group, the  $|M_z = \pm 1/2\rangle$  lower state Zeeman sublevels are depopulated by optical pumping, creating "holes" in the atomic velocity distributions of the two states. Consequently,

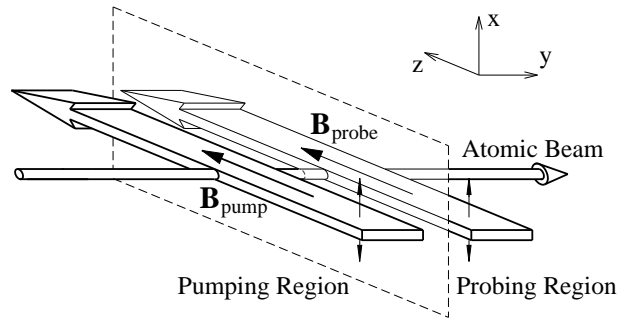


FIG. 2: Conceptual two-region experimental arrangement with separated optical pumping and probing regions used to treat Bennett structure effects in NMOR. Pump and probe light beams are initially linearly polarized along  $x$ , the atomic beam propagates in the  $\hat{y}$  direction, and the magnetic fields are oriented along the direction of light propagation ( $\hat{z}$ ).

there are sub-Doppler features (with minimum width  $\gamma_0$ ) in the indices of refraction  $n^-$  and  $n^+$  for right- and left-circularly polarized ( $\sigma^-$  and  $\sigma^+$ , respectively) light. In the probe region [Fig. 3 (b)], a small magnetic field  $\mathbf{B}_{\text{probe}} < \hbar\gamma_0/(2g\mu)$  is applied. (The Landé factor for the upper state is assumed to be negligible.) The indices of refraction  $n^-$  and  $n^+$  are displaced relative to each other due to the Zeeman shift, leading to optical rotation of the probe beam. In the absence of Bennett structures, this gives the linear Faraday effect. When Bennett holes are produced in the pump region, the resultant Faraday rotation can be thought of as rotation produced by the Doppler-distributed atoms without the hole (linear Faraday rotation) minus the rotation that would have been produced by the pumped out atoms. Thus the rotation due to Bennett holes has the opposite sign to that due to the linear effect. Since the Bennett features are much narrower than those due to the Doppler distribution, the magnetic field  $B_{\text{max}}$  at which rotation of the largest magnitude is seen is accordingly much smaller (occurring when the Zeeman splitting is equal to the linewidth), than for the linear effect.

Light polarization also acquires ellipticity due to Bennett structures in this example. However, since the induced ellipticity is due to differences in the imaginary parts of the indices of refraction, rather than the real parts, it has a dispersive spectral shape whose integral over frequency is zero. Thus induced ellipticity is suppressed relative to the rotation angle by a factor  $\sim \Gamma_D/\gamma_0$ .

Next we discuss a similar setup that produces quite different results. Consider again the same experimental arrangement (Fig. 2) and an  $F = 1/2 \rightarrow F' = 1/2$  transition where the upper state decays to levels other than the lower state; however, now there is the same magnetic field in both pump and probe regions,  $\mathbf{B}_{\text{pump}} = \mathbf{B}_{\text{probe}}$ . In this case, as it turns out, there is no Bennett-structure-related magneto-optical rotation. This is because the identical, sub-Doppler features in the indices of refraction

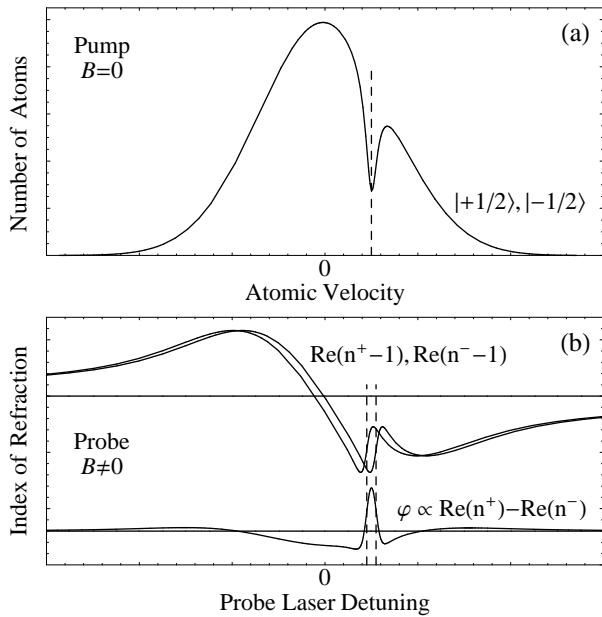


FIG. 3: The Bennett-structure effect on an  $1/2 \rightarrow 1/2$  transition where the upper state decays to levels other than the lower state;  $\mathbf{B}_{\text{pump}} = 0$ ,  $\mathbf{B}_{\text{probe}} \neq 0$ . (a) In the pump region, monochromatic laser light produces Bennett holes in the velocity distributions of atoms in the lower state  $|+1/2\rangle$ ,  $|-1/2\rangle$  sublevels. Since there is no magnetic field, the holes occur in the same velocity group (indicated by the dashed line) for each sublevel. (b) In the probe region, a magnetic field is applied, shifting  $n^+$  and  $n^-$  relative to each other (upper trace). The real part of the indices of refraction are shown; so that the features in plot (a) correspond to dispersive shapes in this plot. The shifted central detunings of the BSR features are indicated by the dashed lines. Polarization rotation of the probe laser light is proportional to the difference  $\text{Re}(n^+) - \text{Re}(n^-)$  (lower trace). Features due to the Doppler distribution and the Bennett holes can be seen. Since the Bennett related feature is caused by the removal of atoms from the Doppler distribution, the sign of rotation due to this effect is opposite to that of the linear rotation.

tion for  $\sigma^-$  and  $\sigma^+$  light created by hole burning in the pump region [Fig. 4 (a)] have the same central frequency in the probe region [Fig. 4 (b)]. Thus the Bennett structures cause no enhanced difference between the indices of refraction for  $\sigma^-$  and  $\sigma^+$  light.

Finally, consider the case of an  $F = 1/2 \rightarrow F' = 1/2$  transition, where the upper state primarily decays back to the lower state, and there is the same magnetic field in both pump and probe regions. The resonant velocity groups for  $\sigma^-$  and  $\sigma^+$  light are different. In the velocity group resonant with  $\sigma^-$  light, atoms are pumped from the  $|M_z = 1/2\rangle$  to the  $|M_z = -1/2\rangle$  state (creating a Bennett hole in the velocity distribution of atoms in the  $|M_z = 1/2\rangle$  state and a Bennett peak in the velocity distribution of atoms in the  $|M_z = -1/2\rangle$  state), while the opposite occurs for atoms in the velocity group resonant with  $\sigma^+$  light [Fig. 5 (a)]. The identical features in the indices of refraction for left- and right-circularly

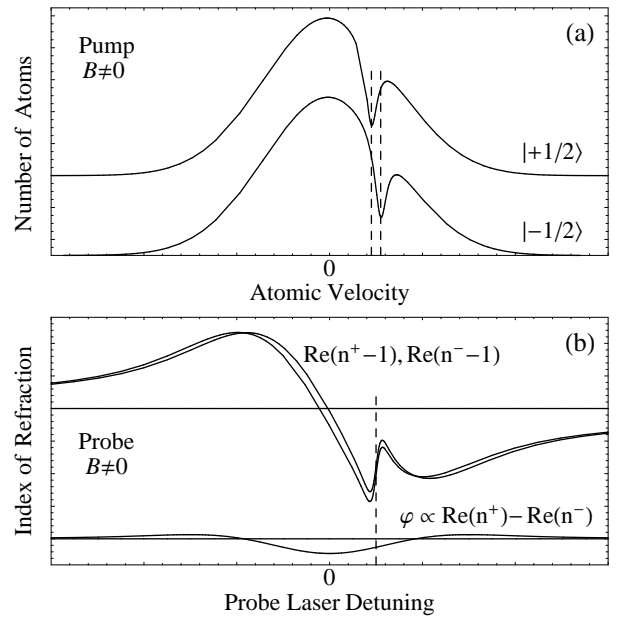


FIG. 4: The Bennett-structure effect on an  $1/2 \rightarrow 1/2$  transition where the upper state decays to levels other than the lower state;  $\mathbf{B}_{\text{pump}} = \mathbf{B}_{\text{probe}}$ . (a) In the pump region, monochromatic laser light produces Bennett holes in the velocity distributions of atoms in the lower state  $|+1/2\rangle$ ,  $|-1/2\rangle$  sublevels. Because a magnetic field is present, different velocity groups (indicated by the dashed lines) are resonant with the pump light for each of the sublevels. (b) In the probe region, since the same magnetic field is present, the features in  $n^+$  and  $n^-$  (upper trace) due to the Bennett holes occur at the same frequency (indicated by the dashed line). Thus there is no BSR feature in the rotation shown in the lower trace).

polarized light due to hole burning occur at the same frequency, so in the probe region there is no optical rotation due to hole burning. However, the peaks due to repopulation occur at shifted frequencies and do cause optical rotation in the probe region [Fig. 5 (b)]. Since peak building increases the number of atoms in the resonant velocity groups, the sign of the rotation is now the *same* as that due to the linear Faraday effect, contrary to the case with  $\mathbf{B}_{\text{pump}} = 0$ ,  $\mathbf{B}_{\text{probe}} \neq 0$ .

These last two cases, where  $\mathbf{B}_{\text{pump}} = \mathbf{B}_{\text{probe}}$ , are analogous to the common experimental case of a single laser beam used for both pumping and probing. Figure 1 shows the magnetic field dependence of Faraday rotation for the  $J = 1 \rightarrow J = 0$  (571 nm) transition in atomic samarium under the conditions of the experiment described in Ref. [9] (single laser beam, laser power  $\approx 5 \mu\text{W}$ , beam diameter  $\approx 1$  mm, no buffer gas). Previous density matrix calculations have been performed for this system [18, 19], showing good agreement with the data. Since both pumping and probing occur in the presence of the magnetic field, for this system, the Bennett-structure-related effects are due to peak building, and thus produce rotation of the same sign as the linear effect. Note

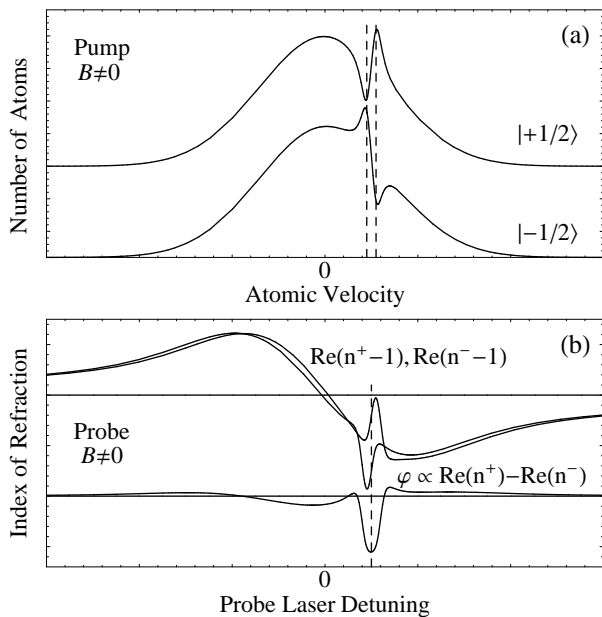


FIG. 5: The Bennett-structure effect on an  $1/2 \rightarrow 1/2$  transition where the upper state decays back to the lower state;  $\mathbf{B}_{\text{pump}} = \mathbf{B}_{\text{probe}}$ . (a) In the pump region, laser excitation and spontaneous decay in the presence of a magnetic field transfers atoms in resonant velocity groups (indicated by the dashed lines) from one lower state sublevel to the other, producing Bennett peaks and holes. (b) In the probe region, since the same magnetic field is present, the features in  $n^+$  and  $n^-$  due to the Bennett *holes* occur at the same frequency (indicated by the dashed line), and thus produce no rotation. However, the features due to the Bennett *peaks* (which partially overlap the features due to the holes) occur at shifted frequencies and *do* produce rotation. Since this nonlinear feature is the result of adding atoms to the Doppler distribution, its sign is the same as that of the linear effect. Note that the width of this BSR feature is greater than that of the feature shown in Fig. 3 (b), since the separation of the peaks is greater than the separation of the holes in Fig. 3 (b).

that it is possible to have BSR NMOR due to hole burning in a single beam experiment. For example, for a  $J = 0 \rightarrow J = 1$  transition under the same conditions, with some upper state decay to other levels, BSR NMOR is caused by two holes burned in the lower state velocity distribution due to the Zeeman splitting of the upper level. In this case BSR NMOR would have the opposite sign as that of the linear effect, as was observed with the 639 nm transition in Sm [9].

### III. BENNETT-STRUCTURE-RELATED NEOE IN SIMPLE SYSTEMS

Nonlinear optical effects analogous to those discussed above also arise for atomic samples in static electric fields due to quadratic Stark shifts of Zeeman sublevels. Consider the experimental geometry shown in Fig. 6. Electric

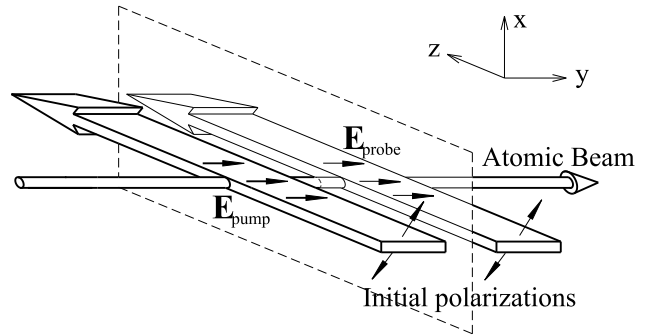


FIG. 6: Conceptual two-region experimental arrangement with separated optical pumping and probing regions used to treat Bennett-structure-related NEOE. Pump and probe light beams are initially linearly polarized in the  $x$ - $y$  plane at  $45^\circ$  to the  $x$ -axis, the static electric fields are oriented in the  $\hat{y}$  direction, atomic beam propagates in the  $\hat{y}$  direction, and light propagates in the  $\hat{z}$  direction.

fields can be applied in the  $\hat{y}$ -direction in both the pump ( $\mathbf{E}_{\text{pump}}$ ) and probe ( $\mathbf{E}_{\text{probe}}$ ) regions. Light propagates in the  $\hat{z}$  direction and both pump and probe beams are initially linearly polarized along an axis in the  $(x, y)$  plane, at  $45^\circ$  to the electric fields. The pump beam is of saturating intensity ( $\kappa \gg 1$ ) and the probe beam is weak ( $\kappa \ll 1$ ). The polarization of the probe beam is analyzed after it has interacted with the atomic sample.

Consider an isolated  $F = 1 \rightarrow F' = 0$  transition, where we choose the quantization axis along the  $\hat{y}$  direction (Fig. 7). The (initially) linearly polarized pump and probe light can be decomposed into  $x$ - and  $y$ -polarized light. The quadratic Stark effect causes a relative shift in the resonance frequency for  $y$ -polarized light compared to that for  $x$ -polarized light. Thus the indices of refraction for near-resonant  $x$ - and  $y$ -polarized light are different. A linear electro-optical effect arises in this case since as near-resonant light propagates through the atomic medium,  $y$ -polarized light changes its phase relative to the  $x$ -polarized light, so as the light propagates through the medium it acquires ellipticity due to linear birefringence. The major axis of the polarization ellipse also rotates with respect to the initial axis of linear polarization due to linear dichroism. However, the roles of the real and imaginary parts of the index of refraction are reversed compared to the case of NMOR discussed in the previous section. Thus in this case, Doppler broadening suppresses optical rotation relative to ellipticity by a factor of  $\sim \Gamma_D/\gamma_0$ .

As discussed in Sec. II, the formation of Bennett structures in the atomic velocity distribution creates sub-Doppler features in the refractive indices. In close analogy with BSR NMOR, the central frequencies of these features are affected by the presence of electric fields in the pump and probe regions, leading to nonlinear electro-optically-induced ellipticity. The physical mechanisms causing BSR-induced ellipticity are exactly analogous to those for the BSR NMOR described in Sec. II, where  $\sigma^+$

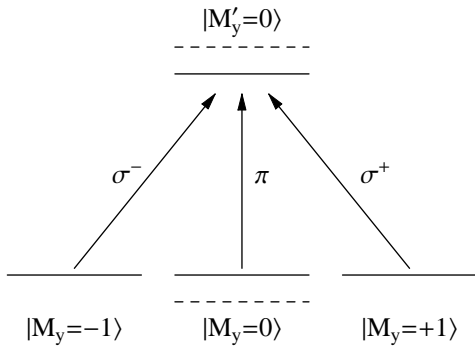


FIG. 7: Level diagram for  $F = 1 \rightarrow F' = 0$  transition. In the presence of an electric field along the quantization axis ( $\hat{y}$ ), the  $M_y = 0$  Zeeman sublevels are shifted by the Stark effect (dashed lines). As a result there arises a difference in the resonance frequencies for  $x$ -polarized ( $\pi$ ) and  $y$ -polarized light (which can be represented as a superposition of  $\sigma^\pm$  light).

and  $\sigma^-$  light polarizations are replaced by  $x$  and  $y$  polarizations. For example, if  $\mathbf{E}_{\text{pump}} = 0$  and  $\mathbf{E}_{\text{probe}} \neq 0$  and the upper state of the transition decays to levels other than the lower state, hole-burning induces ellipticity of the *opposite* sign compared to that caused by the linear electro-optic effect. If  $\mathbf{E}_{\text{pump}} = \mathbf{E}_{\text{probe}}$  and the upper state decays primarily back to the lower state, peak-building induces ellipticity of the *same* sign as from the linear effect.

#### IV. EXPERIMENTAL MEASUREMENTS OF BSR NMOR FOR THE RUBIDIUM D2 LINE

The setup for measurement of Bennett-structure-related NMOR (also described in Ref. [2]) is shown in Fig. 8. The beam from an external cavity diode laser system (EOSI 2010 with central wavelength  $\sim 780$  nm), attenuated with crossed film polarizers, passes through a prism polarizer that produces linearly polarized light. The beam then passes through an uncoated cylindrical vapor cell (2.5 cm diam.  $\times$  7.5 cm long, manufactured by EOSI) inside two layers of magnetic shielding (CONETIC AA alloy). Residual magnetic fields are less than  $\sim 0.1$  mG in any direction. The cell contains a natural mixture of Rb isotopes (72%  $^{85}\text{Rb}$ , 28%  $^{87}\text{Rb}$ ) and no buffer gas (this is important because the presence of buffer gas degrades the effect due to velocity-changing collisions and pressure broadening). In order to eliminate effects related to back-reflection of laser light from the cell windows, the cell is tilted slightly with respect to the direction of light propagation. A magnetic coil that can provide a uniform magnetic field along the direction of light propagation is installed inside the inner magnetic shield. Next, the beam is split by a polarizing beam splitter (PBS) whose axis is rotated by  $45^\circ$  with respect to the axis of the polarizer; the two resulting beams fall onto photodiodes. This *balanced polarimeter* is sen-

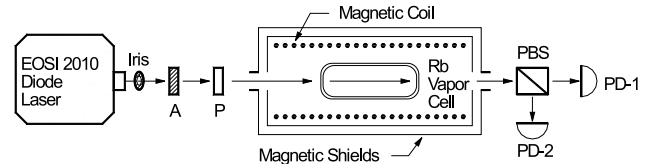


FIG. 8: Schematic diagram of experimental setup for NMOR measurements. A - attenuator, P - linear polarizer, PBS - polarizing beamsplitter used to measure polarization rotation, PD-1,2 - photodiodes.

sitive to the rotation of the plane of linear polarization while being insensitive to changes in ellipticity. Optical rotation data are taken by tuning the laser through resonance and recording the signal from the photodiodes. Transmission through the Rb vapor is proportional to the sum of the photodiode signals  $S_1$ ,  $S_2$ , while the rotation angle [20], in the small angle approximation, is given by

$$\varphi = \frac{S_1 - S_2}{2(S_1 + S_2)}. \quad (1)$$

Figure 9 shows the transmission and optical rotation spectra for a magnetic field of 2.0 G along the light propagation direction. Light power is  $560 \mu\text{W}$ , beam diameter is  $\sim 8$  mm. Bennett-structure-related NMOR for the  $^{87}\text{Rb}$   $F = 2$  and  $^{85}\text{Rb}$   $F = 3$  components reaches a maximum at this value of the magnetic field. (Bennett-structure-related NMOR for the  $^{87}\text{Rb}$   $F = 1$  and  $^{85}\text{Rb}$   $F = 2$  components reaches a maximum at a higher magnetic field. In addition, the contributions from the transit effect and linear effects partially cancel rotation for these components.) For comparison, the results of a density matrix calculation of optical rotation and transmission are also shown in Fig. 9. Our density matrix calculation has been previously described in Ref. [21]. Atomic density ( $\sim 10^{10}$  atoms/cm $^3$ ) and frequency scaling are first determined by comparing theoretical transmission with experiment. The theory assumes one transit rate of atoms through the laser beam, rather than a distribution; this effective rate is determined by the experimental magnetic field dependence of rotation to be  $\approx 0.011 \times 2\pi$  MHz. The theory also assumes a uniform laser light intensity within an effective beam diameter; the effective beam diameter for this data set, 7 mm, is determined by matching the theory to several data sets taken at different laser powers. Discrepancies on the order of 10% between data and theory may be due to these approximations, or to frequency-dependent background rotation.

#### V. EXPERIMENTAL MEASUREMENTS OF BSR NEOE FOR THE RUBIDIUM D2 LINE

The experimental setup for measurement of Bennett-structure-related NEOE is shown in Fig. 10. It is based on the apparatus used in our earlier work [3, 7] with

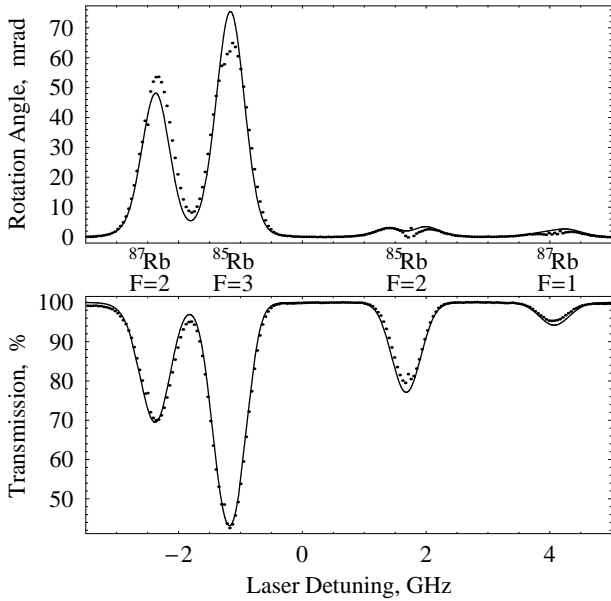


FIG. 9: Upper plot compares an experimental measurement of Bennett-structure-related magneto-optical rotation on the Rb D2 line with  $B = 2.0$  G (dots) to a density matrix calculation (solid line). Lower plot shows both experimental and theoretical transmission spectra. See text for discussion.

a number of significant modifications. For this experiment, a cylindrical, paraffin-coated cell [22] containing both  $^{85}\text{Rb}$  and Cs (length  $\approx 2$  cm, diameter  $\approx 5$  cm) is used. A cell of this type may be employed in a search for the permanent electric dipole moment (EDM) of Cs (see, e.g., [23–26, 7]), where Rb would be used as a “co-magnetometer.” In view of this application, we have presently investigated Bennett-structure-related NEOE as a tool for measuring electric fields inside the cell. The copper electrodes are placed inside a 3D magnetic coil (not shown in Fig. 10), that in turn is placed inside a four-layer magnetic shield (discussed in detail in Ref. [7]). In the experiment, residual magnetic fields are compensated to  $< 0.1 \mu\text{G}$ . An external-cavity diode laser (EOSI 2010) with central wavelength  $\sim 780$  nm is used to produce light near-resonant with the Rb D2 line. The light passes through a linear polarizer oriented at  $45^\circ$  to the direction of the applied electric field. After the light passes through the cell, the degree of ellipticity  $\epsilon$  (equal to the arctangent of the ratio of the minor and major axes of the polarization ellipse [20]) is determined by a circular analyzer consisting of a quarter-wave plate with fast axis along  $y$ , a polarizing beam splitter, and two photodiodes used in differential mode. In the small angle approximation  $\epsilon$  is given by the right-hand side of Eq. 1.

Electric fields of up to 10 kV/cm are applied to the cell. Figure 11 shows the spectrum of induced ellipticity for the  $^{85}\text{Rb}$  D2 line when 10 kV is applied between electrodes, nominally corresponding to an electric field of 5 kV/cm in the cell. The actual field could, in princi-

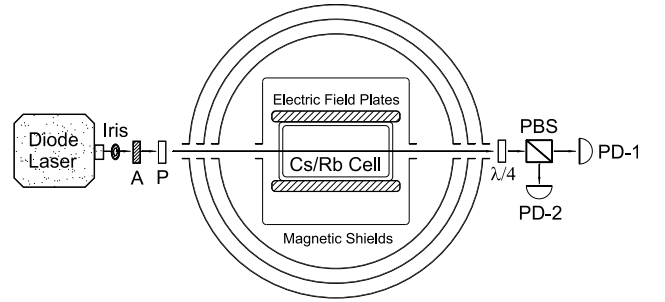


FIG. 10: Schematic diagram of experimental setup for NEOE measurements. A - attenuator, P - linear polarizer,  $\lambda/4$  - quarter-wave plate, PBS - polarizing beamsplitter, PD-1,2 - photodiodes. The relative sizes of the shields, electrodes, and the cell are not to scale.

ple, be affected by redistribution of charges on the glass and paraffin. In addition, the use of a paraffin-coated cell introduces significant complications into the theory, due to the fact that polarized atoms can undergo many thousand collisions with the cell walls without becoming depolarized. The results of a “naive” calculation, which ignores this effect, are compared with the data. We expect this calculation to reproduce qualitative features of the effect, since collisions with the walls, while preserving polarization, do change velocity, and thus destroy Bennett structures. The experimental light power is  $3.5 \mu\text{W}$  and the laser beam diameter is  $\approx 1$  mm, implying a nominal transit rate of  $0.03 \times 2\pi$  MHz (these values are used in the calculation). The density of  $^{85}\text{Rb}$  is determined from the transmission spectrum to be  $\approx 10^9$  atoms/cm $^3$ , somewhat lower than the saturated density at room temperature ( $20^\circ\text{C}$ ) [27]. (It should be noted that we have observed changes in the atomic density ( $\sim$  factor of 2) when the amplitude of the electric field is altered. This effect is currently under investigation, and the results will be reported elsewhere.) Using an electric field of 5 kV/cm in the theory gives reasonable agreement with the data. However, preliminary results from a more realistic calculation that includes the effects of polarization preservation, velocity mixing, and spin exchange indicate that corrections on the order of 50% are generated by these effects, presumably due to more efficient optical pumping of the atoms into “dark” states. Thus the extensions to the theory (to be described in a future work) are needed in order to extract accurate measurements of the electric field.

The quadratic Stark shifts for the upper state of the D2 transition are much larger than those in the lower state, since the total electronic angular momentum  $J$  is  $1/2$  for the lower state (so Stark shifts in this state arise only due to the hyperfine interaction). Calculations indicate that the measured ellipticity in Fig. 11 is primarily due to Bennett structures, and not coherence effects (rotation due to which peaks at a higher value of electric field than that due to Bennett structures in this case) or the linear electro-optical effect. Additionally, we have checked that

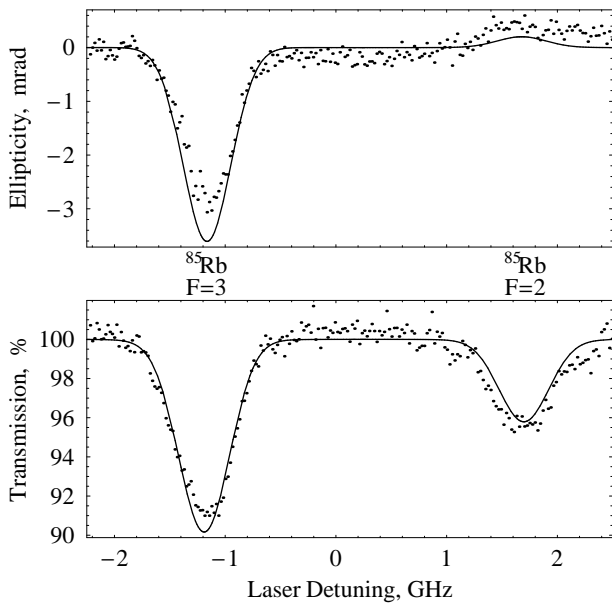


FIG. 11: Upper plot compares a measurement of electric-field-induced ellipticity (at 5 kV/cm, nominally) to a density matrix calculation. Lower plot shows the experimental and theoretical transmission spectra. See text for discussion.

induced ellipticity for the D1 transition is less than 0.1 mrad for an electric field of  $\sim 5$  kV/cm. This is further evidence that the effect observed on the D2 line is primarily due to the formation of Bennett structures and not coherence effects, since coherence effects for the D1 and

D2 transitions are expected to be of similar magnitudes, while the Bennett structure effects are considerably suppressed for the D1 line, since both upper and lower states have  $J = 1/2$ .

## VI. CONCLUSION

In conclusion, we have analyzed nonlinear magneto- and electro-optic effects arising from Bennett structures in the atomic velocity distribution. Considerations of the effects in systems with low angular momentum indicate that depending on the transition and the experimental geometry, either “hole burning” or “peak building” can be the primary mechanism for nonlinear optical effects. By comparing measurements of Bennett-structure-related magneto-optical rotation and electric-field-induced ellipticity to density matrix calculations, we have demonstrated that density matrix calculations provide a quantitative description of Bennett-structure-related nonlinear optical effects. We have performed the first detailed investigation of Bennett-structure-related nonlinear electro-optic effects, and have demonstrated that they can be used for electric field measurements.

## Acknowledgments

We are grateful to M. Zolotarev for helpful discussions. This research has been supported by the Office of Naval Research, grant N00014-97-1-0214.

- 
- [1] W. Gawlik, in *Modern Nonlinear Optics*, edited by M. Evans and S. Kielich, Advances in Chemical Physics Series Vol. LXXXV, Pt. 3 (Wiley, New York, 1994).
- [2] D. Budker, D. J. Orlando, and V. Yashchuk, *Am. J. Phys.* **67**, 584 (1999).
- [3] D. Budker, V. Yashchuk, and M. Zolotarev, *Phys. Rev. Lett.* **81**, 5788 (1998).
- [4] D. Budker, D. F. Kimball, S. M. Rochester, V. V. Yashchuk, and M. Zolotarev, *Phys. Rev. A* **62**, 043403 (2000).
- [5] L. M. Barkov, M. S. Zolotarev, and D. Melik-Pashayev, *Sov. JETP Pis'ma* **48**, 144 (1988).
- [6] B. Schuh, S. I. Kanorsky, A. Weis, and T. W. Hansch, *Opt. Commun.* **100**, 451 (1993).
- [7] V. Yashchuk, D. Budker and M. Zolotarev, in *Trapped Charged Particles and Fundamental Physics*, edited by D. H. E. Dubin and D. Schneider (American Institute of Physics, New York, 1999), pp. 177-181.
- [8] D. Macaluso and O. M. Corbino, *Nuovo Cimento* **8**, 257 (1898); *Ibid.* **9**, 384 (1899).
- [9] L. M. Barkov, D. Melik-Pashayev, and M. Zolotarev, *Opt. Commun.* **70**, 467 (1989).
- [10] W. R. Bennett, *Phys. Rev.* **126**, 580 (1962).
- [11] D. Budker, D. F. Kimball, S. M. Rochester, and V. V. Yashchuk, *Phys. Rev. Lett.* **85**, 2088 (2000).
- [12] V. A. Sautenkov, M. D. Lukin, C. J. Bednar, I. Novikova, E. Mikhailov, M. Fleischhauer, V.L. Velichansky, G. R. Welch, and M. O. Scully, *Phys. Rev. A* **62**, 023810 (2000).
- [13] I. Novikova, A. B. Matsko, V. A. Sautenkov, V. L. Velichansky, G. R. Welch, and M. O. Scully, *Opt. Lett.* **25**, 1651 (2000).
- [14] R. Müller and A. Weis, *Appl. Phys. B* **66**, 323 (1998).
- [15] I. O. G. Davis, P. E. G. Baird, and J. L. Nicol, *J. Phys. B: At. Mol. Opt. Phys.* **21**, 3857 (1988).
- [16] S. V. Fomichev, *J. Phys. B: At. Mol. Opt. Phys.* **28**, 3763 (1995).
- [17] D. Budker, D. F. Kimball, S. M. Rochester, and V. V. Yashchuk, Preprint LBNL, Pub-5453, Berkeley, California, 1999 (available at <http://socrates.berkeley.edu/~budker/>).
- [18] M. G. Kozlov, *Opt. Spectrosc. (USSR)* **67**(6), 789 (1989).
- [19] K. P. Zetie, R. B. Warrington, M. J. D. Macpherson, and D. N. Stacey, *Opt. Commun.* **91**, 210 (1992).
- [20] S. Huard, *Polarization of Light* (Wiley, New York, 1997). Note that the angle of ellipticity  $\epsilon$  and the polarization angle  $\varphi$  are related to the Stokes' parameters  $P_i$  by  $P_3/P_0 = \sin 2\epsilon$  and  $P_2/P_0 = \cos 2\epsilon \sin 2\varphi$ .
- [21] S. M. Rochester, D. S. Hsiung, D. Budker, R. Y. Chiao,

- D. F. Kimball, and V. V. Yashchuk, Phys. Rev. A **63**, 043814 (2001).
- [22] E. B. Alexandrov, M. V. Balabas, A. S. Pasgalev, A. K. Vershovskii, and N. N. Yakoson, Laser Phys. **6**, 244 (1996).
- [23] E. S. Ensberg, Phys. Rev. **153**, 36 (1967).
- [24] S. A. Murthy, D. Krause, Z. L. Li, and L. R. Hunter, Phys. Rev. Lett. **63**, 965 (1989).
- [25] L. R. Hunter, Science **252**, 73 (1991).
- [26] I. B. Khriplovich and S. K. Lamoreaux, *CP Violation without Strangeness. The Electric Dipole Moments of Particles, Atoms and Molecules* (Springer-Verlag, Berlin, 1997).
- [27] *Handbook of Physical Quantities*, edited by I. S. Grigoriev and E. Z. Meilikhov (CRC Press, Boca Raton, FL, 1997).